Cross Mark

Fabrication of a New Dye-Sensitized Solar Cell Using CuO/TiO$_2$ Nanocomposite Synthesized via an Electrochemical Technique

Ali A. Ahmed[1]* and Aqeel M. JreoAlduhaidahawi[2]
[1]*Ministry of Education, Rusafa Second Directorate of Education, Baghdad, Iraq.*
[2]*Department of Chemistry, College of Science, Kufa University, Najaf, Iraq.*
Corresponding Author Email: alia.alhussaini@student.uokufa.edu.iq

----

Abstract
Various standard methods have previously been used for the synthesis of nanoparticles that produce unhealthy waste. They are also considered unsafe and expensive methods. An alternative technology is needed to synthesize nanoparticles that consume less energy and are more environmentally friendly. In this research, a CuO/TiO$_2$ nanocomposite has been synthesized with a mole ratio of 1.5:1, which produces good energy and no environmental pollution using an easy and fast method (electrochemical). The morphology and structure of the nanocomposite were examined using TEM, FESEM, AFM, and FTIR. The particle size of the CuO/TiO$_2$ nanocomposites was found to range between 10.52 and 88.10 nm, while optical properties were diagnosed using UV-visible spectroscopy since its measurements showed the amount of gap energy (3.08 eV). The structure of the nanocomposite was demonstrated using X-ray diffraction (XRD), where the mixed anatase and rutile phases were observed for TiO$_2$, while the monoclinic (tenorite) phase was observed for CuO. Additionally, dye-sensitized solar cells (DSSCs) have been fabricated from CuO/TiO$_2$ nanocomposite, which was synthesized by a new green method, and pigments (methylene blue as a chemical dye and chlorophyll as a natural dye). These DSSCs were characterized by their high ability to absorb ultraviolet energy, where the efficiency of energy conversion η of ITO-CuO/TiO$_2$ was approximately 2.62 and 3.87% with chlorophyll (a natural dye) and methylene blue (a chemical dye), respectively, where η of ITO-CuO/TiO$_2$ with methylene blue is the best.

Keywords: DSSCs, Electrochemical, Nanocomposites, Copper Oxide, Titanium dioxide

----

Introduction

The increasing demand for energy due to the depletion of natural energy sources in the world leads to a trend towards renewable energy through the exploitation of solar energy, wind energy, waterfall energy, etc. Solar cells are a promising and important technology and are the future of sustainable energy for humans. The solar cells installed in cars are capable of absorbing solar energy to replace the traditional use of diesel and gas.

Using the same principle, solar energy can also charge cell phones. There are such a wide variety of applications [1]. The goal of this study was to fabricate a solar cell from nanocomposite and dyes with high sensitivity to light (dye-sensitized solar cells) and produce electrical energy with high efficiency, low cost, and environmental friendliness compared to other types of solar cells [2]. In dye-sensitized solar cells (DSSCs), dye is used

to harvest light and produce electrons, while titanium dioxide (TiO_2) mimics carbon dioxide's role in photosynthesis [3]. An important parameter affecting the efficiency of the cell is the dye's absorption on the surface of nanoparticles [4]. DSSCs consist of wideband semiconductors, selective dye, a conducting electrolyte, and two electrodes with opposite charges [5]. In addition, sensitizer dye is crucial to the functioning of DSSC, and semiconductor materials that fulfil these properties are TiO_2, ZnO, and CuO [6]. Since TiO_2 resists degradation under ultraviolet light, it remains the preferred material among these materials [7]. The chemical absorption of pigment on nanoparticles of CuO and TiO_2 plays an important role in solar cell efficacy [8]. Natural dyes found in the leaves of plants, flowers, fruits, and vegetables can replace conventional dyes without a noticeable loss in effectiveness [9]. The low cost of dye, availability, biodegradation capability, non-toxicity, and efficiency make it suitable for application as dye-sensitized [10]. TiO_2 and transition metal oxide can be mixed to make composites like ZnO/TiO_2 [11] and Cu_2O/TiO_2 [12] that are much more photocatalytically active. CuO nanoparticles were used to create p-DSSC photocathodes that have a larger valence band gap and a higher dielectric constant [13]. There are several ways to create the CuO/TiO_2 nanocomposite powder, such as electrochemical precipitating, co-precipitation, sol-gel precipitation, solution combustion, and solid-state reactions. The electrochemical precipitating method, which is used in this work, produces nanocomposites quickly, easily, cheaply, and with high purity [14]. In this study, chlorophyll (a natural dye) and methylene blue as a chemical dye were utilized to generate electricity by applying photovoltaic solar cells. The reason for choosing methylene blue (MB) is that it is cheap, available, easy to prepare, and does not cause harm to humans. It has been used as a sunscreen for human skin to reduce UV damage [15]. The maximum absorption wavelength of MB is 665 nm. As well as its strong absorption power, photon absorption allows visible light to be carried by the dye as the electron transfers to the CuO/TiO_2 nanocomposites [16]. On the other hand, chlorophyll is a green dye found in green plant leaves due to their capacity to absorb red and blue light. It has the greatest absorption at wavelength 675 nm. Furthermore, it contains three carboxylate groups in a molecule without heavy metal ions and is regarded as an environmentally friendly photosensitizer [17].

Materials and Methods
Chemical and Reagents

All materials and solvents utilized in this search were used as such without further purification, whereas titanium foil (99%) and copper foil (98%) were obtained from Baoji Jinsheng Metal Material Company, LTD, (China) potassium chloride (96%) and polyvinyl alcohol (PVA) were supplied from Fluka Company (Switzerland), graphite electrodes were obtained from Graphite India Limited (India), acetone (98%), ethanol (99%), polyethene glycol (PEG, 97%), and potassium iodide (97%) were provided by CDH (China), iodine (99%) was obtained from Thomas Baker & CO Limited (England), deionized water (DW) was obtained from OneMed (Sweden), methylene blue dye (98%) was obtained from Alfa Aesar (United States), natural eucalyptus leaves and Indium Tin Oxide (ITO) glass (76.2 × 25.4 × 1.1 mm, 11–15 Ω) were obtained from Redox Me Company (Sweden).

Instrumentation

CuO/TiO_2 was characterized using UV-Vis (Shimadzu UV-1650, Japan), FTIR (Shimadzu 8400, Japan), FESEM (INSPECT F50,

Germany), AFM (Naio, Nanosurf AG, Switzerland), TEM (EM 208S, USA), XRD (PANalytical AERIS, UK), EDX (Thermo Axia ChemiSEM, USA), and Power Supply (UNI-T UTP3345TD, China).

Methods
Preparation of CuO / TiO$_2$ nanocomposites

The CuO/TiO$_2$ nanocomposite was synthesized by the electrochemical method using the active electrode (anode), which is an electrode made of copper and titanium foil, and the inert electrode (cathode), which is a graphite electrode, as shown in Fig.1.

Figure 1. **Electrochemical apparatus used to prepare the CuO/ TiO$_2$ nanocomposites**

A power source was also used. The anode and cathode were cleaned with ethanol and acetone before being rinsed with DW [18]. The electrochemical cell was filled with a 200.0 mL electrolyte solution consisting of 5 mL of 10% (w/v) KCl and 10 mL of 10% (w/v) PVA (stabilizer agent), and the remaining volume of the electrolyte solution was filled with deionized water. In addition, the active electrode consisted of connected pieces of copper foil (0.75 cm × 4 cm) and titanium foil (1 cm × 4 cm), which were placed face-to-face with a graphite electrode (2 cm × 5 cm) and subsequently immersed in the cell electrolyte [19]. The electrolysis process was carried out in an undivided electrolytic cell and stirred at 30 °C for about 60 min at 25 V. The CuO/TiO$_2$ precipitate resulting from this process was centrifuged, rinsed several times with ethanol absolute and DW, and then placed in a drying oven where it was dried for about 60 min at 70 °C before being calcined at 700 °C for around 60 min [20].

Fabrication of dye-sensitized solar cells (DSSCs)

ITO glass was carefully cleaned with ethanol and DW before being dried with air to remove impurities. The following method was used to design a chemically and naturally dye-sensitive solar cell: A few drops of PEG were added to a small amount of CuO/TiO$_2$ nanocomposite to make a colloidal solution (photoanode). While the counter electrode was made of graphite powder and a few drops of PEG, the photoanode and the counter electrode were annealed at 300 °C for around 2 hours. The photoanode was placed in a chemical dye solution of 0.5% (w/v) MB by the same method, but another photoanode was put in a chlorophyll dye solution extracted from eucalyptus leaves [21]. Then, both electrodes are placed in the dark for about 7–12 hours. Then, it is cleaned using ethanol and DW. Finally, 2–3 drops of an electrolyte solution of 0.1 M iodine (10 g of KI and 3.715 g of I$_2$ in 250 mL DW) were placed between the two electrodes, and the solar cell efficiency was determined [22]. Fig. 2 shows the schematic diagram and design of DSSCs.
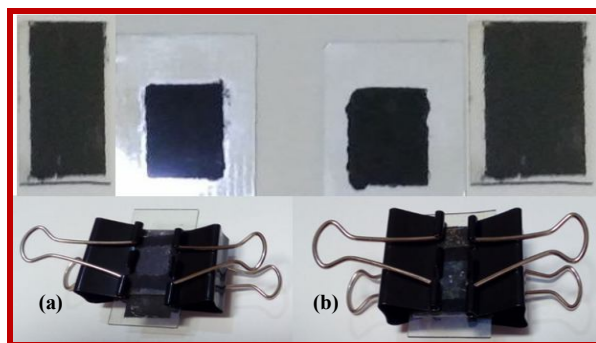
Figure 2. **Design of chemical (a) and natural dye DSSCs (b)**

The working principle of DSSC is initiated as follows: (1) The dye molecules adsorbed on the semiconductor photoanode start to absorb the solar light. (2) The electrons in the excited state are injected into the conduction band (CB) of the semiconductors to produce an electric current. Then the current travels through the external wire and is collected by the transparent conductive substrate of the counter electrode. (3) The oxidized dye is regenerated by the redox system in the electrolyte solution. (4) The redox system is regenerated through a counter-electrode. It can be observed that an efficient electron transfer mechanism in the DSSCs can be obtained if the energy level of each component is properly aligned. For example, the energy level of the lowest unoccupied molecular orbital (LUMO) of the dye must be higher than the CB of CuO/TiO_2. Whereas the CB of the CuO/TiO_2 photoanode must be above the redox potential of the electrolyte. Similarly, the redox potential of the electrolyte must be above the highest occupied molecular orbital (HOMO) level of the dye. Fig. 3 highlights the electron transfer mechanisms and their energy.
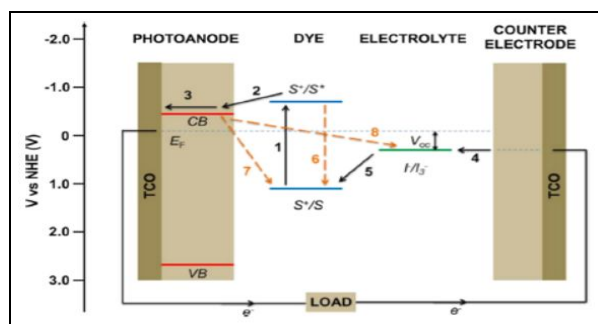
Figure 3. Electron transfer mechanisms and energy level diagram of DSSCs

The details and explanations are highlighted as follows**:**

Mechanism 1 (Photoexcitation)

After the adsorption of a photon (hv) by the photosensitizer (dye), the dye molecules change from the ground state, S, into the excited state, S*, or excite an electron from the HOMO level to the LUMO level through the following reaction.

$$S_{adsorbed} + hv \rightarrow S_{*adsorbed} \qquad (1)$$

Mechanism 2 (Electron injection)

Then the excited dye molecules will inject the electrons into the CB of the semiconductor, thus leaving the dye in an oxidized state, S+, as follows:

$$S_{*adsorbed} \rightarrow S_{*adsorbed} + e\text{- injected} \qquad (2)$$
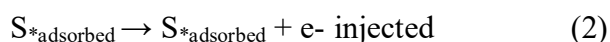
Mechanism 3 (Energy generation)

The injected electrons are transmitted through the semiconductor (CuO/TiO_2 film), and ultimately the electrical energy is transferred through the conductive substrate, an external circuit, and a counter electrode. This highly efficient process usually occurs in milliseconds (ms).

$$e\text{-injected} + C.E \rightarrow e\text{-}C.E + \text{electrical energy} \qquad (3)$$

It is crucial to note that electron transport occurs by diffusion due to the electron concentration that becomes the main driving force for electron transport in the CuO/TiO_2 mesoporous film. Furthermore, incident light intensity plays an important role in determining whether faster electron diffusion can be obtained at higher light intensities.

Mechanism 4 (Reduction of redox mediator)

In the 4th mechanism, the I3 in the electrolyte that obtains an electron will reduce to I− at the counter electrode. Thus, the regenerative cycle is complete.

$$I_3 + 2.e\text{-}C.E \rightarrow 3I\ C.E \qquad (4)$$

Mechanism 5 (Regeneration of dye)

At the same time, the oxidized dyes, S+, are shifted to the ground-state dye, S, caused by the electron obtained from I−, and thus the regenerative cycle is completed.

$$S^+_{adsorbed} + 3/2\ I \rightarrow S_{adsorbed} + 1/2\ I_3 \qquad (5)$$

Mechanism 6 (Recombination)

Direct recombination of the excited dye is reflected by the excited state lifetime.

Mechanism 7 (Recombination)

The next recombination process is the injection of electrons into the CuO/TiO$_2$ with oxidized dyes.

$$S+_{adsorbed} + e\text{-}CuO:TiO2 \rightarrow S_{adsorbed} \qquad (6)$$
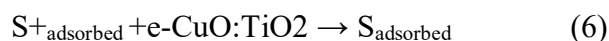
Mechanism 8 (Recombination)

Lastly, the recombination of injected electrons in the CuO/TiO$_2$ with acceptors in the electrolyte [23].

$$I_3 + 2.e\text{-}CuO:TiO2 \rightarrow 3I\ (anode) \qquad (7)$$
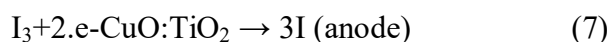
Results and Discussion

X-Ray Diffraction Analysis for CuO/ TiO$_2$ Nanocomposites

The XRD patterns of the CuO/TiO$_2$ nanocomposite revealed an overlap between the peaks located in the same or neighboring region for both TiO$_2$ NPs and CuO NPS, while some peaks appear isolated where there is no overlap between them. As well, these peaks are different in intensity, as shown in Fig. 4. The diffraction peaks at 2θ° 25.40°, 27.51°, 36.15°, 41.26°, 44.11°, 46.35°, 53.55°, 54.36°,56.72°, 62.76°, 64.14°, and 69.02° related to the Miller indices (101), (110),

(101), (210), (111), (200), (105), (211), (220), (213), (310), and (116), respectively represent the anatase and rutile phases of TiO$_2$ (JCPDS No. 89-4921) [24], while other peaks appeared at 2θ° 32.60°, 35.72°, 38.80°, 48.81°, 51.37°, 58.37°, 61.61°, 66.32°, 68.15°,72.43°, and 75.02° associate to the Miller indices (110), (002), (111), (-202), (020), (202), (-113), (-311), (220), (311), and (222), respectively confirm the monoclinic (tenorite) structure of CuO (JCPDS card no. 48-1548) [25]. The relative broad peaks at 2θ 27.51°, 53.55°, and 54.36° were indexed to the diffraction of the TiO$_2$ planes (110), (105), and (211), and the broad peaks at 2θ 35.72°, 38.80°, 48.81°, 66.32°, and 68.15° were indexed to the diffraction of the CuO planes (002), (111), (-202), (-113), and (220), demonstrating that TiO$_2$ and CuO coexist in the CuO-TiO$_2$ heterojunction. Therefore, it is concluded that the anatase-rutile TiO$_2$ lattice constants are identical to those of the monoclinic (tenorite) CuO [26]. Consequently, the CuO/TiO$_2$ nanocomposites were produced by decreasing the intensity of diffraction angles in some peaks and increasing them in other peaks. Through the XRD technique, the average composite size of CuO/TiO$_2$ nanocomposites can be calculated using Scherrer's (Eq. 8), where it was 32.89 nm because the variables of this equation obtained XRD data:

$$D = K\lambda/\ FWHM\ cos\ \Theta \qquad (8)$$
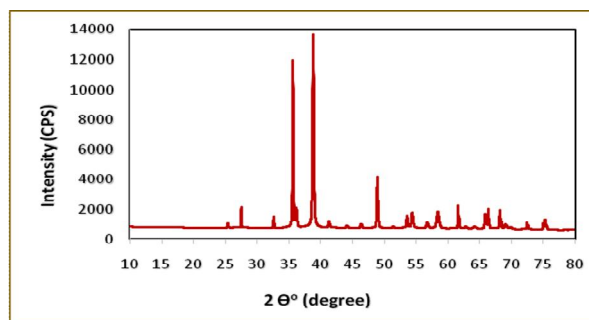
Figure 4. **X-Ray diffraction pattern of CuO/ TiO$_2$ nanocomposites**

Where D is the size of the crystals, θ is the Bragg diffraction angle, FWHM is the full width of the diffraction peak at half maximum, λ is the wavelength of Cu-K radiation (0.15406 nm), K is a constant, and it is equivalent to 0.9 [27].

TEM Analysis for CuO/TiO$_2$ Nanocomposites

The transmission electron microscopy (TEM) micrographs of the CuO/TiO$_2$ nanocomposites provide evidence of the CuO nanoparticle's regular and homogeneous rectangular and cubic morphology. Moreover, the TiO$_2$ nanoparticles had a spherical morphology and very small diameters. Additionally, it was found that some of the TiO$_2$ nanoparticles adhered to the CuO surface, while others were embedded in the CuO nanoparticles, which is illustrated in Fig. 5, and these findings are consistent with Ravishankar et al. results [28]. Statistical results showed that the mean particle sizes of CuO/TiO$_2$ nanocomposites at 100 nm and 50 nm scales were 31.04 and 18.21 nm, respectively. This is additional evidence for the preparation of CuO/TiO$_2$ nanocomposites.
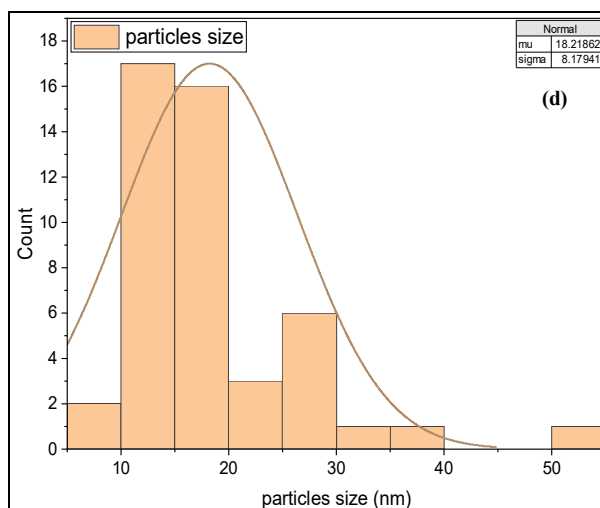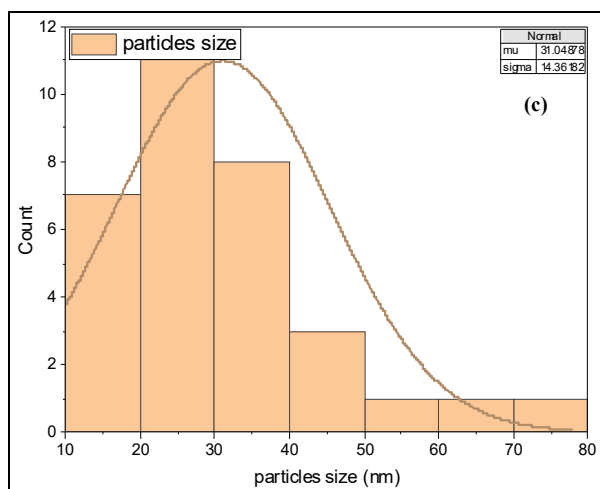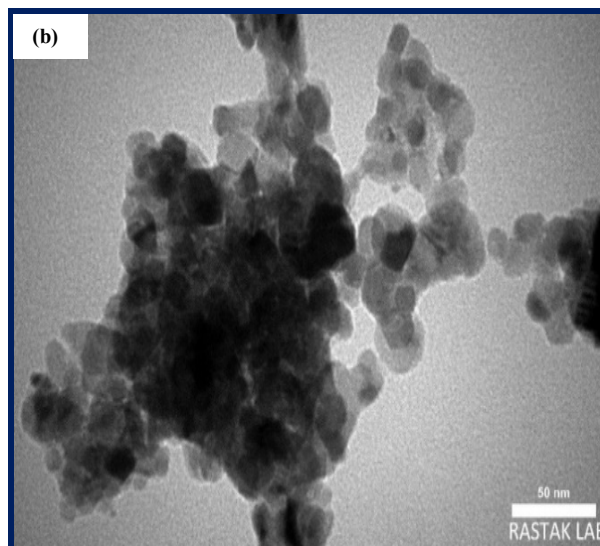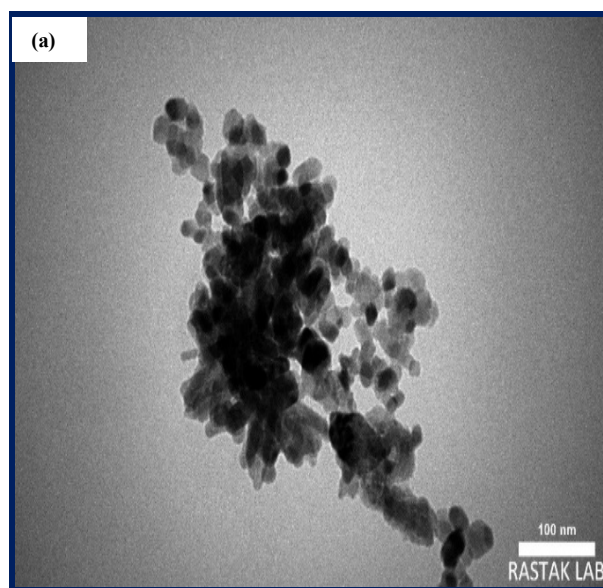
Figure 5. TEM images and size distribution graphs of CuO/TiO$_2$ nanocomposites at different scales (a, c) at 100 nm and (b, d) at 50 nm

FESEM Analysis for CuO/ TiO$_2$ Nanocomposites

The morphology of CuO/TiO$_2$ nanocomposites was observed using FESEM. Fig. 6 indicates that the nanoparticles were prepared in the nanometer range, and some of the nanoparticles are well separated from each other. while most of it was present in the agglomerated form of tiny crystals. This agglomeration is due to the electrostatic effects, which reveals that this agglomeration behavior of nanoparticles is consistent with a behavior similar to the agglomeration of nanoparticles in previous studies [29]. It also provides evidence of CuO nanoparticle cubes while producing a flower-like morphology. While the TiO$_2$ nanoparticles had a spherical morphology and very small diameters, statistical results showed that the mean particle sizes of CuO/TiO$_2$ nanocomposites at 500 nm and 5 µm were 82.84 nm and 0.798 µm, respectively.
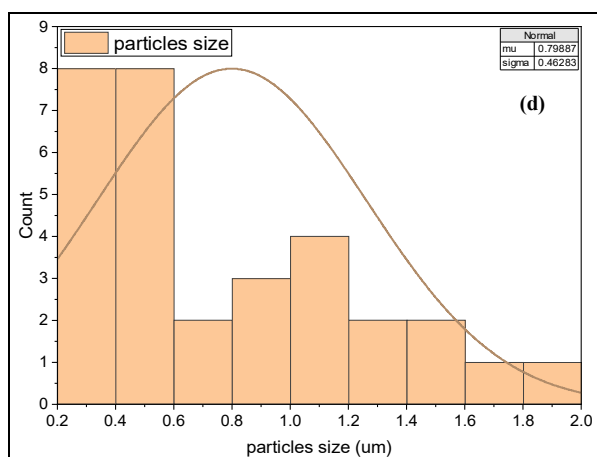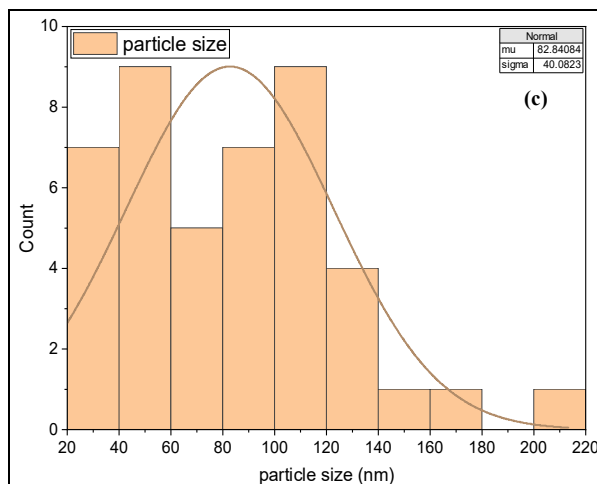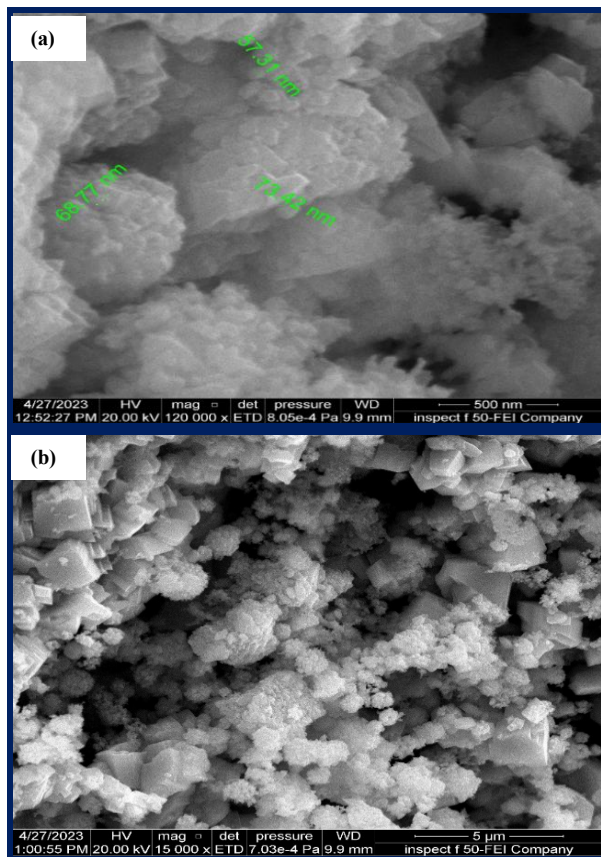
Figure 6. **FESEM images and size distribution graphs of CuO/TiO$_2$ nanocomposites at different scales (a, c) at 500 nm, and (b, d) at 5 µm**

EDX AnalysisforCuO/ TiO$_2$ Nanocomposites

The purity, confirmed composition, distribution of the elements in the samples, and stoichiometry of the electrochemically produced CuO/TiO$_2$ nanocomposites were evaluated using energy-dispersive X-ray spectroscopy (EDX). Fig. 7 revealed the presence of unique signals for oxygen, copper, and titanium and confirmed that there was a high level of purity in the samples. The mole ratio of CuO/TiO$_2$ is (Cu = 18.7%, Ti = 12.7%, O = 50.1%), and the weight percentages of CuO/TiO$_2$ are (Cu = 42.2%, Ti = 21.5%, O = 28.4%). These ratios demonstrate that the ratio of CuO to TiO$_2$ was 1.5:1.
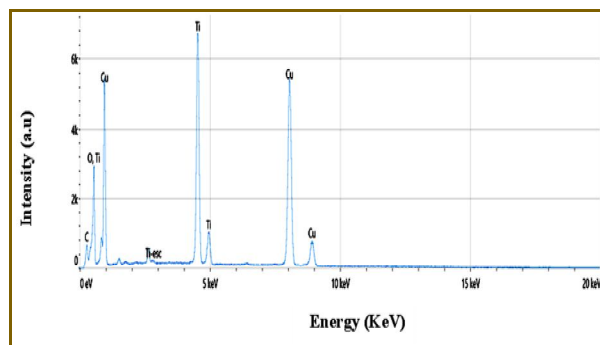
Figure 7. **EDX spectrum of CuO/ TiO₂ nanocomposites**

AFM Analysis for CuO/ TiO₂ Nanocomposites

The nanocomposites of CuO and TiO$_2$ were diagnosed using AFM. The morphology observed indicates that the surface 3D consists of an aggregation of granules called clusters; this indicates good homogeneity, as shown in Fig. 8. This surface topography is essential for many applications, notably photodetector responsivity. The measurements included a mean diameter of 44.70 nm, a mean height of 3.468 nm, and roughness analyses such as root mean square (Sq) of 3.022 nm, limit maximum height (Sz) of 42.08 nm, arithmetic mean height (Sa) of 1.647 nm, and a surface area ratio (Sar) of 1.610. On the other hand, AFM measurements supply excellent information on the size distribution, homogeneity of nanoparticle surfaces, and the mean diameter of nanoparticles [30].
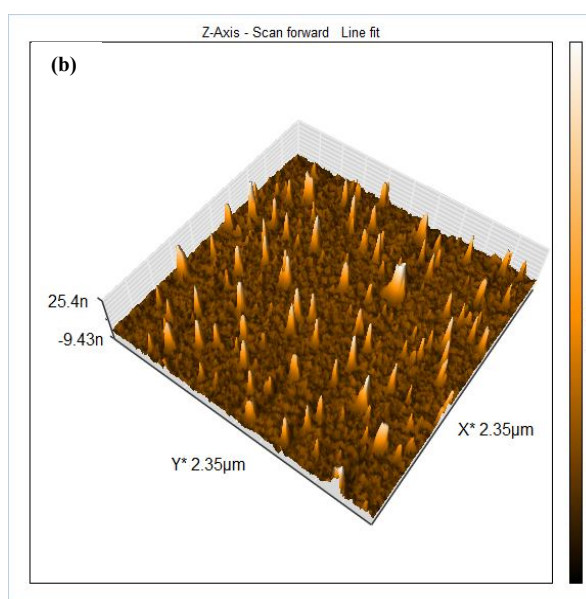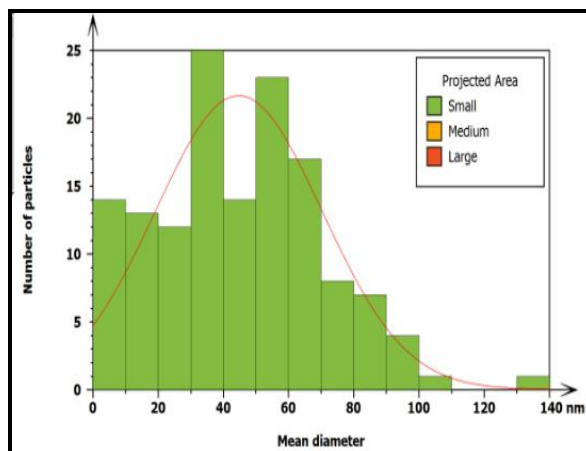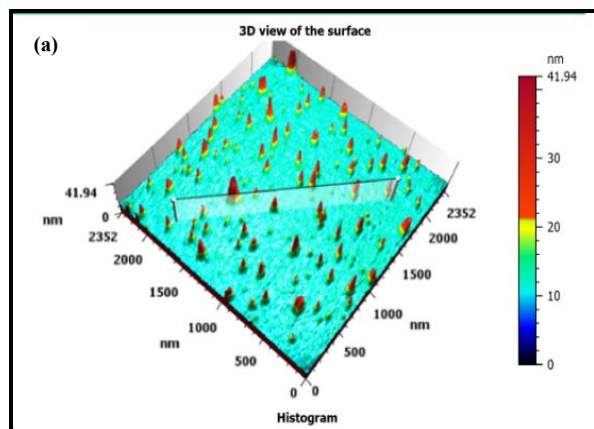
Figure 8. **AFM (a) particle analysis, and (b, c) 3D image scales of CuO/ TiO₂ nanocomposites**

UV-vis study of CuO/ TiO₂ nanocomposite

Nanocomposite thin films of CuO and TiO₂ were made on glass slides at room temperature and analyzed with solid-state UV-visible spectroscopy. Fig. 9(a) shows the λmax obtained was around 402 nm, and the energy band gap was calculated by the Tauc. relation (Eq. 9) [31].

$$\alpha h\nu^{1/n} = k(h\nu - E_g) \qquad (9)$$

where K is a constant, α is the molar extinction coefficient, $h\nu$ is the incident photon energy in eV, E_g is the optical energy band gap, and n: index depends on the type of transition. The band gap was estimated from the intersection of the two lines part of $(\alpha h\nu)2$ Plots vs. $h\nu$ on the $h\nu$ axis. The equation is a direct band gap. Based on this equation, the bandgap value of CuO/TiO₂ is 3.084 eV, as shown in Fig. 9(b), which indicates that CuO/TiO₂ is a semiconductor because the calculated energy gap value of 3.084 eV is less than 4.0 eV [32].
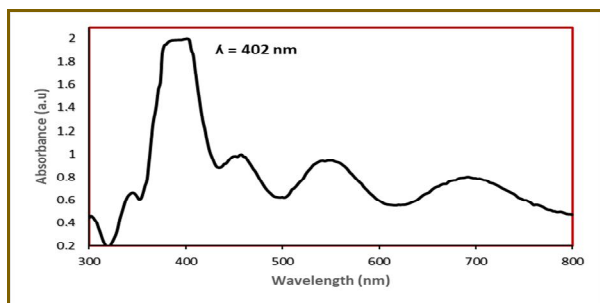
Figure 9(a). **UV-Vis Spectrum of CuO/ TiO₂ nanocomposites**
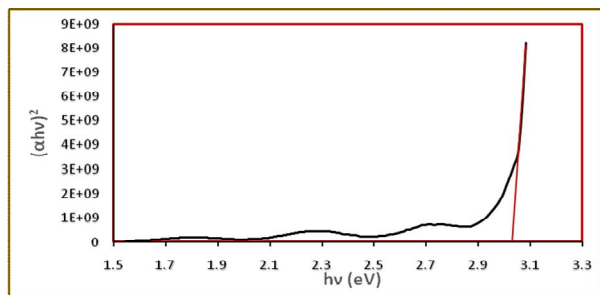
Figure 9(b). **Tauc plot graph of the optical band gap energy of CuO/TiO₂nanocomposites**

FTIR Analysis for CuO/TiO₂ Nanocomposite

Fourier transmission infrared (FTIR) spectroscopy is an efficient technique to show the functional groups of the CuO/TiO₂ nanocomposites Fig. 10. shows the stretching vibrations of the hydroxyl group (OH) in CuO/TiO₂ (metal hydroxyl and/or the hydroxyl of water molecules of crystallization) ranged between 3446-1637 cm⁻¹, while the stretching vibrations of the metal-metal oxides Cu-Ti-O and Ti-O-Ti ranged between 580-503 cm⁻¹, and 484-441 cm⁻¹, respectively, while the stretching vibrations were for the metal oxides Cu-O and Ti-O ranged between 891-534 cm⁻¹, and 765-441 cm⁻¹, respectively. Numerous well-defined peaks can be observed [33].
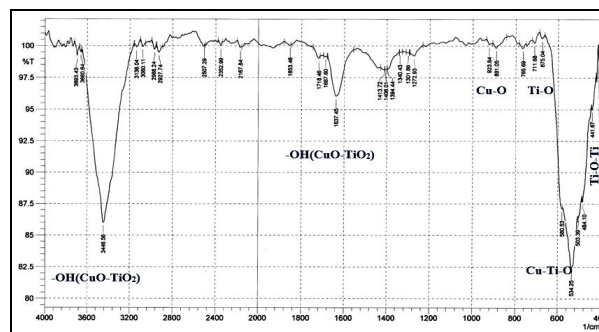
Figure 10. **FTIR Spectrum of CuO/ TiO₂ nanocomposites**

Applications
The DSSCs Parameter

The following formula (Eq. 10) was used to calculate the solar cell's energy conversion efficiency (η):

$$\eta = p_{max}/p_{in} = (V_{oc} \cdot J_{sc} \cdot FF)/p_{in}) \times 100\% \qquad (10)$$

where p max is the maximum power output, Voc is a photovoltaic open circuit, Jsc is short circuit density, and Pin is a lamp power incident, which is equal to 40 mW/cm². Additionally, the fill factor (FF) is represented by (Eq. 11):

FF= Vmax. Jmax/Voc. Jsc   (11)

where Jmax is the current density and Vmax is the maximum output voltage. The characteristics of the solar cell are Voc = 0.62, 0.65 V, Jsc = 5, 7.3 mA/cm^2, Vmax = 0.35, 0.36 V, Jmax = 3, 4.3 mA/cm^2, FF = 0.338, 0.326, and the conversion efficiency is 2.62, 3.87 % for CuO/TiO$_2$ with chlorophyll and MB dyes, respectively. One important aspect of introducing dyes is the improvement in the absorbance of visible light resulting from the synergistic effect of CuO/TiO$_2$ nanocomposite and MB that could efficiently suppress charge recombination, improve interfacial charge transfer, enhance visible-light adsorption, and provide plentiful photocatalytic reaction active sites. The solar efficiency of using chlorophyll a and chlorophyll b dyes that absorb at 649 nm and 665 nm, respectively, is attributed to auxochrome groups, such as carbonyl (C=O) groups, which supply the ability to absorb light in a visible spectrum from the sun. Thus, these auxochrome groups can be connected to the Cu (II) and Ti (IV) positions of the CuO/TiO$_2$ surface in favor of electron transfer from the chlorophyll molecules to the CuO/TiO$_2$ conduction band. In addition, chlorophylls possess a porphyrin ring, which serves as a suitable light-harvesting antenna for assembling solar energy. Consequently, CuO/TiO$_2$ with porphyrin has been a good sensitizer for achieving photocatalysis of visible light [34]. While enhancing solar efficiency by the use of chemical dye (MB) is due to the occurrence of an electron transfer from the dye into CuO/TiO$_2$ nanocomposite, and the results showed higher efficiency of the MB dye compared to the pigment chlorophyll, this was attributed to MB absorbing in three bands, one in the visible region (l max = 665 nm) and two in the UV region (l max = 300 nm and l max = 250 nm).

Additionally, due to the difficulty of fixing the natural dye on the semiconductor surface, as well as the presence of alkyl and vinyl groups in the structure, this causes a steric barrier that prevents chlorophyll molecules from interacting with CuO/TiO$_2$ [35,36]. Fig. 11 shows the J-V curve for the dye-sensitized solar cell, which is based on a synthetic CuO/TiO$_2$ nanocomposite.
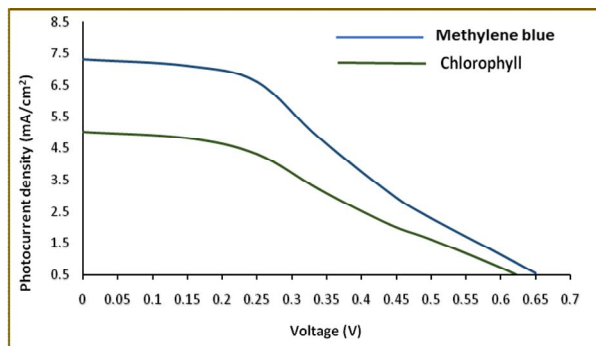
Figure 11. **J-V curve for the dye-sensitized solar cell**

Conclusion

Dye-sensitized solar cells (DSSCs) with high efficiency in producing electrical energy were prepared from CuO/TiO2 nanocomposite from available and cheap raw materials and by a safe, easy, and fast e method. The FESEM, TEM, and AFM images indicated that samples revealed a well-ordered and good-sized distribution of particles, and the outcomes of XRD, TEM, and AFM techniques showed a composite synthesized in a nanoscale size range. Also, the energy band gap was measured using UV-visible techniques, while the stretching vibrations of the metal-metal oxides Cu-Ti-O and Ti-O-Ti ranged between 580-503 cm^{-1}, and 484-441 cm^{-1}, respectively, using FTIR. Dyes with high sensitivity to light were used to improve the efficiency of the cell, where the efficiency of energy conversion η of ITO-CuO/TiO$_2$ was approximately 2.62 and 3.87% with chlorophyll and MB, respectively. This study will serve in the future for the possibility of fabricating more efficient cells from natural materials.

Acknowledgement

Conflict of Interest

The authors declare no conflicts of interest.

References

1. B. O'regan and M. Grätzel, *Nature*, 353 (1991) 737.
https://doi.org/10.1038/353737a0

2. P. Rana, B. Kaushik, K. Solanki, K. M. Saini and R. K. Sharma, *Chem. Commun.*, 58 (2022) 11354.
https://doi.org/10.1039/D2CC03568E

3. B. Vaz and M. Pérez-Lorenzo, *Nanomaterials*, 13 (2023) 1097.
https://doi.org/10.3390/nano13061097

4. S. Koudjina, V. Kumar, G. Y. Atohoun, J. D. Gbenou and P. Chetti, *J. Photochem. Photobiol. A: Chem.*, 442 (2023) 114772.
https://doi.org/10.1016/j.jphotochem.2023.114772

5. R. Chauhan, *Inorg. Chem. Commun.*, 139 (2022) 109368.
https://doi.org/10.1016/j.inoche.2022.109368

6. S. Rahman, A. Haleem, M. Siddiq, M. K. Hussain, S. Qamar, S. Hameed and M. Waris, *RSC Adv.*, 13 (2023) 19508.
https://doi.org/10.1039/D3RA00903C

7. S. Bibi, S. S. Shah, F. Muhammad, M. Siddiq, L. Kiran, S. A. Aldossari, M. S. S. Mushab and S. Sarwar, *Chemosphere*, 339 (2023) 139583.
https://doi.org/10.1016/j.chemosphere.2023.139583

8. T. F. Yadeta and T. Imae, *Appl. Surf. Sci.*, 637 (2023) 157880.
https://doi.org/10.1016/j.apsusc.2023.157880

9. I. C. Maurya, A. K. Gupta, P. Srivastava and L. Bahadur, *Opt. Mater.*, 60 (2016) 270.
https://doi.org/10.1016/j.optmat.2016.07.041

10. A. S. Teja, A. Srivastava, J. A. Satrughna, M. K. Tiwari, A. Kanwade, H. Lee, A. Ogura and P. M. Shirage, *J. Sol. Energy* , 261 (2023) 112.
https://doi.org/10.1016/j.solener.2023.06.004

11. Ji. Lin, Li. Jiaxing, Lei. Jinghua, Ren. Yuanyuan, Zhou. Shuyu and Li. Lihua, *Catal. Commun.*, 174 (2023) 106572.
https://doi.org/10.1016/j.catcom.2022.106572

12. I. Ciria Ramos, E. J. Juarez Perez and M. Haro, *Small*, 28 (2023) 2301244.
https://doi.org/10.1002/smll.202301244

13. T. Jiang, M. Bujoli-Doeuff, Y. Farré, Y. Pellegrin, E. Gautron, M. Boujtita, L. Cario, S. Jobic and F. Odobel, *RSC Adv.*, 6 (2016) 112765.
https://doi.org/10.1039/C6RA17879K

14. E. P. Estévez Ruiz, J. L. Lago and S. P. *Thirumuruganandham, Materials*, 16 (2023) 3076.
https://doi.org/10.3390/ma16083076

15. Z. M. Xiong, X. Mao, M. Trappio, C. Arya, J. E. Kordi and K. Cao, *Sci. Rep.* 11 (2021) 1.
https://doi.org/10.21203/rs.3.rs-150379/v1

16. M. Z. Muzakkar, D. Wibowo and M. Nurdin, *Mater. Sci. Eng.* 267 (2017) 012035.
https://doi.org/10.1088/1757-899x/267/1/012035

17. A. Omar, M. S. Ali and N. Abd Rahim, *Annu. Rev. Sol. Energy* , 207 (2020) 1088.
https://doi.org/10.1016/j.solener.2020.07.028

18. B. Micó-Vicent, E. Perales Romero, J. Jordán-Núñez and V. Viqueira, *Appl. Sci.*, 11 (2021) 5568.

https://doi.org/10.3390/app11125568

19. Y. Y. How, A. Numan, M. N. Mustafa, R. Walvekar, M. Khalid and N. M. Mubarak, *J. Energy Storage*, 51 (2022) 104324.
https://doi.org/10.1016/j.est.2022.104324

20. A. M. El-Khawaga, A. Zidan and A. I. Abd El-Mageed, *J. Mol. Struct.*, 1281 (2023) 135148.
https://doi.org/10.1016/j.molstruc.2023.135148

21. A. Anand, S. Mittal, V. Leeladevi and D. De, *Mater. Today Proc.*, 72 (2023) 227.
https://doi.org/10.1016/j.matpr.2022.07.048

22. A. M. Rheima, D. H. Hussain and H. J. Abed, *IOP Conf. Ser.: Mater. Sci.*, 928 (2020) 052036.
https://doi.org/10.1088/1757-899X/928/5/052036

23. A. Sacco, *Renew. Sustain. Energy Rev.*, 79 (2017) 814.
https://doi.org/10.1016/j.rser.2017.05.159

24. V. S. Benitha, K. Jeyasubramanian and V.S. Prabhin, *Mater. Res. Express*, 9 (2022) 056404.
https://doi.org/10.1088/2053-1591/ac6fbd

25. S. Yu, X. Jia, J. Yang, S. Wang, Y. Li and H. Song, *Mater. Lett.*, 291 (2021) 129531.
https://doi.org/10.1016/j.matlet.2021.129531

26. X. Gou and Z. Guo, *Langmuir*, 36 (2019) 64.
https://doi.org/10.1021/acs.langmuir.9b03224

27. P. Sarkar, Nisha, P. Kumar and R. S. Katiyar, *Chem. Select*, 31 (2023) e202301545.
https://doi.org/10.1002/slct.202301545

28. T. N. Ravishankar, M. D. O. Vaz, S. Khan, T. Ramakrishnappa, S. R. Teixeira, G. R. Balakrishna, G. Nagaraju and J. Dupont, *Chem. Select*, 1 (2016) 2199.

https://doi.org/10.1002/slct.201600068

29. A. Kubiak, Z. Bielan, M. Kubacka, E. Gabała, A. Zgoła-Grześkowiak, M. Janczarek, M. Zalas, A. Zielińska-Jurek, K. Siwińska-Ciesielczyk and T. Jesionowski, *Appl. Surf. Sci.*, 520 (2020) 146344.
https://doi.org/10.1016/j.apsusc.2020.146344

30. V. Kestens, G. Roebben, J. Herrmann, Å. Jämting, V. Coleman, C. Minelli, C. Clifford, P. J. De Temmerman, J. Mast, L. Junjie and F. Babick, *J. Nanoparticle Res.*, 18 (2016) 1.
https://doi.org/10.1007/s11051-016-3474-2

31. J. Tauc, *Mater. Res. Bull.*, 3 (1968) 37.
https://doi.org/10.1016/0025-5408(68)90023-8

32. A. Mancuso, N. Blangetti, O. Sacco, F.S. Freyria, B. Bonelli, S. Esposito, D. Sannino and V. Vaiano, *Nanomaterials*, 13 (2023) 270.
https://doi.org/10.3390/nano13020270

33. L. Gnanasekaran, R. Pachaiappan, P.S. Kumar, T. K. Hoang, S. Rajendran, D. Durgalakshmi, M. Soto-Moscoso, L. Cornejo-Ponce and F. Gracia, *Environ. Pollut.*, 287 (2021) 117304.
https://doi.org/10.1016/j.envpol.2021.117304

34. T. T. Buu, V. H. Son, N. T. Nam, N. D. Hai, H. T. Vuong, N. M. Dat, T. H. Lin, M. T. Phong and N. H. Hieu, *Ceram. Int.*, 49 (2023) 9868.
https://doi.org/10.1016/j.ceramint.2022.11.162

35. S. Krishnan and A. Srivastava, *J. Environ. Chem. Eng.*, 9 (2021) 104699.
https://doi.org/10.1016/j.jece.2020.104699

36. M. R. Munandar, A. S. Hakim, H. A. Puspitadindha, S. P. Andiyani and F. Nurosyid, *J. Phys. Conf. Ser.*, 2190 (2022) 012042.
https://doi.org/10.1088/1742-6596/2190/1/012042